DALTON
FULL PAPER

Structures and properties of 6-aryl substituted tris(2-pyridylmethyl)-amine transition metal complexes

Zhicong He, Donald C. Craig and Stephen B. Colbran *

School of Chemical Sciences, University of New South Wales, Sydney, NSW 2052, Australia

Received 29th July 2002, Accepted 30th September 2002
First published as an Advance Article on the web 22nd October 2002

A series of metal(II) complexes of [6-(2′,5′-dimethoxyphenyl)-2-pyridylmethyl]bis(2-pyridylmethyl)amine (L) have been prepared. X-Ray crystal structures have been determined for L and its metal(II) chloride complexes for Mn, Fe, Co, Ni, Cu and Zn and the results compared. The preparation and crystal structure of the unusual carbonato-bridged copper-tetramer $[Cu_4(L)_4(CO_3)_2][BF_4]_4 \cdot 5.2H_2O$ is also described. The solution-state structures of the complexes are deduced from their physicochemical and spectroscopic properties. The Zn(II) complex, $[ZnCl_2(L)]$, shows inversion about the ligand amine group on the NMR timescale — results from a variable temperature NMR study are presented and allow estimation of the barrier to amine inversion as 56 ± 0.5 kJ mol^{-1}. Overall, it is found that the intramolecular steric interactions introduced by substitution of the tris(2-pyridylmethyl)amine (tpa)-skeleton by a single 6-aryl group result in significant changes to the structures and properties of the resulting metal complexes: in particular the aryl-substitution in L causes (i) a weaker ligand-field compared to tpa favouring high-spin complexes, (ii) a tendency toward lower coordination numbers, and (iii) hemilability in the Ni(II) and Cu(II) complexes — the aryl-substituted leg of the ligand (L) is coordinatively labile.

The potentially tetradentate ligand tris(2-pyridylmethyl)amine (tpa) was first prepared in 1967 by Anderegg and Wenk,[1] and complexes of tpa are now characterised for most metal ions.[1–32] Most recently, iron and copper complexes of tpa and its simple derivatives have risen to special prominence as mimics for biological metal centres, especially those that bind and activate dioxygen.[3–9] The study of these complexes has contributed greatly to understanding of iron–dioxygen and copper–dioxygen chemistries, and has led to new catalysts for oxidation of organic substrates using the clean oxidants, oxygen or hydrogen peroxide.

Substitution of the tpa skeleton has recently emerged as a powerful strategy for changing and controlling the properties of (tpa)metal complexes, including structure, magnetism and, most importantly, stoichiometric and catalytic reactivity.[3–18] To date, simple alkyl substitution of one or more of the tpa pyridines at the 6-position has most often been employed: intramolecular steric interactions in the complexes cause the more highly substituted derivatives to bind metal ions more weakly thus favouring high-spin (iron) complexes or (copper) complexes with "dangling" non-coordinated pyridylmethyl "legs". For example: $[Fe(tpa)(CH_3CN)_2][ClO_4]_2$ is a low-spin iron(II) complex whereas $[Fe(Me_2tpa)(CH_3CN)_2][ClO_4]_2$ and $[Fe(Me_3tpa)(CH_3CN)_2][ClO_4]_2$ are high spin iron(II) species; these are important changes since the spin state of these iron compounds profoundly influences their reactivity, for instance, with organic peroxides.[7] Likewise, copper(I) complexes of alkyl-tpa derivatives exhibit different oxygen reactivities compared to the parent (tpa)Cu(I) compound,[8,9] and different structures and reactivities are found for even the simplest copper(II) complexes — for example whereas trigonal bipyramidal (*tbp*) $[Cu(\kappa^4N\text{-tpa})Cl]^+$ is obtained from copper(II) chloride and tpa,[10] the crystals obtained from Me_3tpa and copper(II) chloride contain a solid solution of square pyramidal (*sp*) $[Cu(\kappa^3N\text{-}Me_3tpa)Cl_2]$ and *sp*-$[Cu(\kappa^4N\text{-}Me_3tpa)Cl]^+$ and its chloride counter ion.[11]

In contrast to alkyl-substitution of tpa, aryl-substitution has been relatively little and only recently exploited. Canary and co-workers have reported the preparations and electrochemical characterisation of the copper(I) complexes, $[Cu(Ph_n tpa)]^+$ (n = 1–3),[12] the X-ray crystal structures of $[Cu(Ph_3tpa)][BPh_4]$ and $[Cu(Ph_3tpa)(MeCN)_2](ClO_4)_2$,[13] copper complexes of tpa derivatives with benzocrown ether substituents as a second (s-block) metal ion binding site,[14] and some cadmium and zinc complexes of chiral ligands based on the tpa skeleton that have phenyl substituents.[15] More recently, Que and co-workers reported that the 6-phenyl-substituent within $[Fe(Phtpa)(MeCN)_2]^{2+}$ is hydroxylated following treatment with *tert*-butylperoxide and base,[16] and Mandon *et al.* demonstrated that 6-(4-methoxyphenyl)-substitution of a tpa-pyridine suffices for that "leg" to be unbound in the ferric chloride ($FeCl_3$) complex.[17] In this contribution, we describe first d-series metal(II) complexes of [6-(2′,5′-dimethoxyphenyl)-2-pyridylmethyl]bis-(2-pyridylmethyl)amine (L) which demonstrate that substitution of the tpa-skeleton by a single aryl substituent is sufficient to significantly change the structures and properties of the resulting complexes.

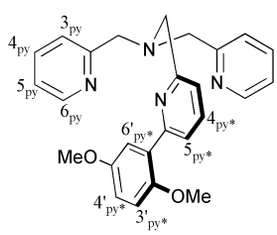

L

Results

Syntheses

Ligand. Ligand L was synthesised by two routes. Both started with monolithiation of 1,4-dimethoxybenzene, reaction of the monolithio product with tri(*iso*-propyl)borate and then hydrolysis with hydrochloric acid to give the arylboronic acid, which was coupled with 6-bromo-2-pyridylcarboxaldehyde under Suzuki conditions to afford 6-(2′,5′-dimethoxyphenyl)-2-

 DOI: 10.1039/b207406k

Table 1 Selected key bond length (Å) and bond angle (°) data for the metal(II) chloride complexes

	$[MnCl_2(L)]$	$[FeCl_2(L)]$	$[CoCl(L)][BPh_4]$	$[Ni_2Cl_2(L)_2]Cl_2$[a]	$[CuCl(L)][PF_6]$	$[ZnCl_2(L)]$
M–Cl1	2.486(1)	2.476(1)	2.262(1)	2.356(1)	2.228(1)	2.234(1)
M–Cl2	2.391(1)	2.328(1)		2.492(1)		2.244(1)
M–N1	2.413(4)	2.360(4)	2.131(4)	2.167(4)	2.509(3)	
M–N2	2.303(5)	2.223(4)	2.077(4)	2.056(4)	1.984(3)	2.193(2)
M–N3	2.300(4)	2.232(4)	2.108(4)	2.094(4)	1.977(3)	2.220(2)
M–N4	2.322(4)	2.235(4)	2.187(3)	2.070(4)	2.051(3)	2.215(2)
Cl1–M–Cl2	104.58(6)	102.55(5)		84.41(4)		115.59(4)
Cl1–M–N1	87.9(1)	87.3(1)	112.1(1)	105.4(1)	105.70(8)	
Cl1–M–N2	159.5(1)	160.6(1)	103.1(1)	99.3(1)	96.1(1)	100.25(7)
Cl1–M–N3	88.4(1)	87.6(1)	95.8(1)	94.9(1)	97.1(1)	101.09(7)
Cl1–M–N4	90.0(1)	89.7(1)	170.3(1)	175.6(1)	174.2(1)	114.59(7)
Cl2–M–N1	120.0(1)	117.1(1)		90.8(1)		
Cl2–M–N2	94.0(1)	94.2(1)		172.8(1)		97.09(7)
Cl2–M–N3	93.7(1)	93.7(1)		90.1(1)		95.79(7)
Cl2–M–N4	159.1(1)	161.9(1)		92.6(1)		129.80(7)
N1–M–N2	75.2(2)	76.3(2)	115.4(2)	94.1(2)	86.5(1)	
N1–M–N3	145.9(1)	149.2(1)	113.8(1)	159.7(2)	96.7(1)	
N1–M–N4	74.7(1)	76.3(1)	76.3(1)	77.7(2)	80.1(1)	
N2–M–N3	99.0(2)	101.2(2)	114.2(2)	83.4(2)	165.0(2)	147.22(9)
N2–M–N4	74.5(2)	76.6(2)	76.4(1)	83.4(2)	83.4(1)	75.01(9)
N3–M–N4	71.4(2)	73.3(2)	75.9(1)	82.0(2)	82.8(1)	73.57(9)

[a] For $[Ni_2Cl_2(L)_2]Cl_2$, Cl2 = Cl^i.

pyridylcarboxyaldehyde (**A**) in 82% overall yield. The first route to L was based on traditional syntheses of tris(pyridylmethyl)-amines and required conversion of **A** to 6-(2′,5′-dimethoxyphenyl)-2-pyridylmethylbromide (**B**), which was achieved by borohydride reduction of **A** and treatment of the intermediary alcohol with phosphorous tribromide. Reaction of **B** and *N*,*N*-bis(2-pyridylmethyl)amine (bpma) in the presence of triethylamine gave L, isolated in 74% yield after chromatography (silica support, dichloromethane eluent). The second route was direct coupling of **A** and bpma using sodium cyanoborohydride and afforded L in near to quantitative yield. Clearly the latter reductive amination is the more convenient route, and it should be readily adaptable to the preparations of other mono-substituted tpa-derivatives.

Metal complexes. The complexes $[MCl_2(L)]$ (M = Mn, Fe and Zn), $[CoCl(L)]_2[CoCl_4]$, $[Ni_2Cl_2(L)_2]Cl_2$ and [CuCl(L)]Cl were prepared in good yield (70–90%) by simply mixing the appropriate metal dichloride and L (1.0–1.05 equivalents) in methanol or ethanol solution. The Fe(II) complex was air-sensitive and was always handled under a nitrogen atmosphere; the product(s) from its oxidation were not investigated. The crystals of $[CoCl(L)]_2[CoCl_4]$ were not of sufficient quality for an X-ray structural analysis and, therefore, were treated with Na-$[BPh_4]$ to give $[CoCl(L)][BPh_4]$. A similar metathesis reaction of [CuCl(L)]Cl with $K[PF_6]$ afforded $[CuCl(L)][PF_6]$. The preparation of the Cu(I) complex $[Cu(L)][BF_4]$ from L and $[Cu(MeCN)_4][BF_4]$ under rigorously anaerobic conditions is described elsewhere.[18] When a clear yellow solution of $[Cu(L)][BF_4]$ was treated with dioxygen in acetone at −40 °C, the solution immediately turned green. When no solid formed on equilibration of this solution with diethyl ether under dinitrogen, the solution was left to evaporate in air. A few crystals of the green tetramer $[Cu_4(L)_4(CO_3)_2][BF_4]_4 \cdot 5.2H_2O$ were obtained.

Crystal structures

The following labelling scheme for the nitrogen donors of L is used throughout the following discussion: N_{py*} for the nitrogen (N1) of the 6-dimethoxyphenyl-2-pyridylmethyl (PY*) leg; N_{py} for the nitrogen (N2 or N3) of a 2-pyridyl (PY) leg; N_{am} for the amine nitrogen (N4). Key bond length and angle data from the structures of the complexes are presented in Table 1.

Ligand L. Fig. 1 shows the molecular structure of L. The three pyridylmethyl legs are *anti*- with respect to N_{am} and

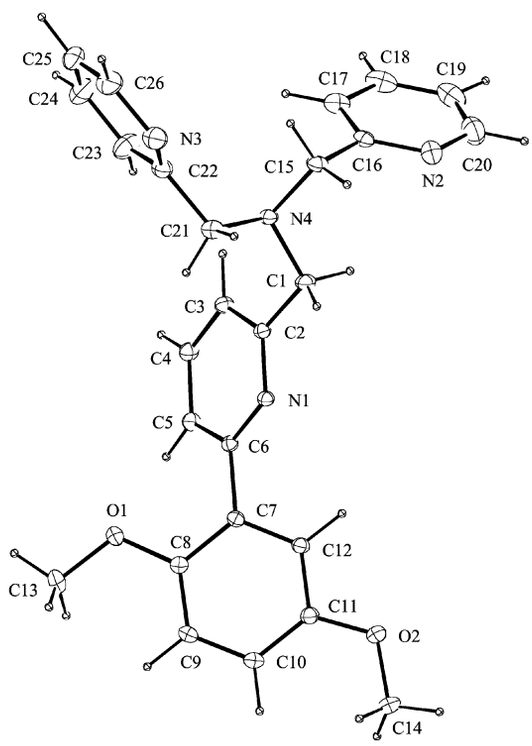

Fig. 1 View of L showing the 10% thermal ellipsoids at 294 K.

splayed outward from the approximate C_3 symmetric axis that the molecule would have if the dimethoxyphenyl substituent were ignored. The geometry minimises interactions between the nitrogen lone pairs. Likewise, the methoxy groups of the PY* leg are oriented away from the tpa-core and the twist about the dimethoxyphenyl–pyridine inter-annular bond is 24°.

$[MCl_2(L)]\cdot MeOH$ (M = Mn, Fe). The Mn(II) and Fe(II) complexes are isomorphous, co-crystallising with methanol in the orthorhombic space group Pna_{21}. In the crystal structures, the only significant intermolecular interaction is the hydrogen bond between the lattice methanol and a chloride ancillary ligand [Mn: Cl2···O1Me 3.16(4) Å; Fe: Cl2···O1Me 3.158(6) Å] of the $[MCl_2(L)]$ (M = Mn, Fe) complex, *e.g.* Fig. 2. The metal(II) centres are in distorted octahedral environments bound by the

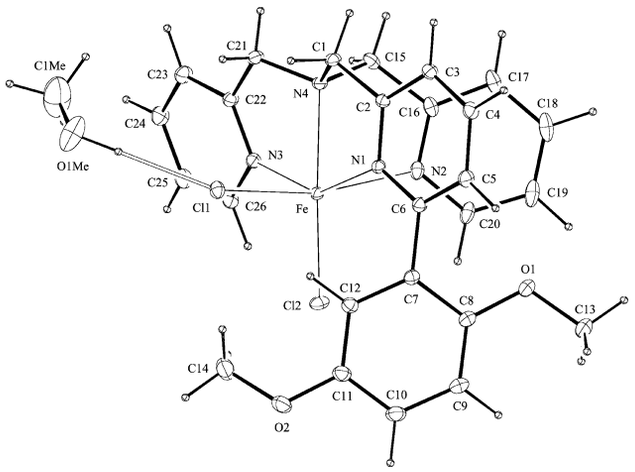

Fig. 2 View of $[FeCl_2(L)]\cdot MeOH$ showing the 10% thermal ellipsoids at 294 K.

four nitrogens of L and two chloride co-ligands. The distortion from ideal octahedral coordination geometry is imposed by L, for example the average N_{am}–M–$N_{py/py*}$ angle is 73.5° for $[MnCl_2(L)]$ and 75.4° for $[FeCl_2(L)]$, and results in acute Cl1–M–N2, Cl2–M–N4 and N1–M–N3 angles (along the octahedral axes) of 159.5(1)°, 159.1(1)° and 145.9(1)° for $[MnCl_2(L)]$ and 160.6(1)°, 161.9(1)° and 149.2(1)° for $[FeCl_2(L)]$. The M–N bond lengths for both complexes, Table 1, are indicative of high-spin [Mn(II): $S = {}^5/_2$; Fe(II): $S = 2$] species, as is confirmed by their magnetic properties (see below). For each complex, the dimethoxyphenyl–pyridine inter-annular twist is 48° and the M–N_{py*} bond [Mn: 2.413(4) Å; Fe: 2.360(4) Å] is significantly longer than the other M–N bonds (av. Mn–$N_{py/am}$: ~2.31 Å; av. Fe–$N_{py/am}$: ~2.23 Å); the latter distances are comparable to those previously found in octahedral high-spin M(II) complexes of tpa and derivatives, *e.g.* 2.205–2.366 Å in $[Mn_2(tpa)_2(ca)][ClO_4]_2$ (ca = dianion of chloranilic acid),[19] 2.18–2.25 Å in $[Fe(6\text{-}Me_3tpa)(CH_3CN)_2]^{2+}$,[7] 2.14–2.255 Å in $[Fe_2(O_2CCH_3)_2(tpa)_2F_2]^{2+}$,[20] 2.17–2.23 Å in $[Fe(6\text{-}Me_3tpa)(bf)]^+$ (bf = benzoylformate)[21] and average ~2.165 Å in $[Fe_2Cl_2(tpa)_2][BPh_4]_2$.[22] The structures of $[MCl_2(tpa)]$ (M = Mn, Fe) are not available for comparison.†

[CoCl(L)][BPh_4]. The crystal structure of [CoCl(L)][BPh_4] reveals a slightly distorted trigonal bipyramidal coordination geometry for the Co(II) ion ($\tau^{33} = 0.92$) with the three pyridyl groups in the equatorial plane and the amine and a chloride co-ligand in the apical positions, Fig. 3 and Table 1. The Co–N_{py*} bond length [2.131(4) Å] is not significantly larger than the Co–N_{py} bond lengths [av. 2.095 Å]; to achieve this the dimethoxyphenyl–pyridyl inter-annular twist increases to *ca.* 65°. Constrained by the ligand L, the N_{am}–Co–$N_{py/py*}$ angles average 76.2° and consequently the Co(II) ion appears "displaced" by *ca.* 0.45 Å from the equatorial plane toward the chloride co-ligand; the Co–N_{am} distance is 2.187(3) Å. An analogous (tpa)Co(II) complex is unknown; the reported examples of Co(II) complexes of tpa are all octahedral.[23–25]

$[Ni_2(\mu\text{-}Cl)_2(L)_2]Cl_2\cdot MeOH\cdot 5H_2O$. Each Ni(II) ion in this centrosymmetric dimer sits in a distorted octahedral N_4Cl_2-coordination environment, Fig. 4. The two nickel ions are separated by 3.59 Å, asymmetrically bridged by two chloride

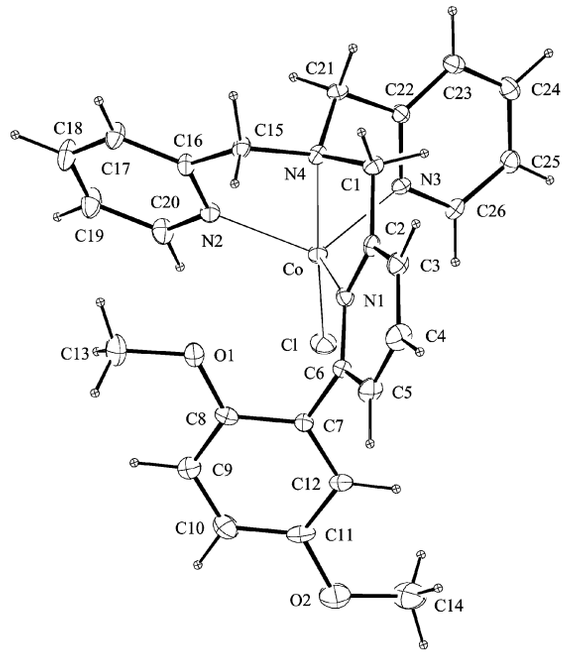

Fig. 3 View of the $[CoCl(L)]^+$ ion showing the 10% thermal ellipsoids at 294 K.

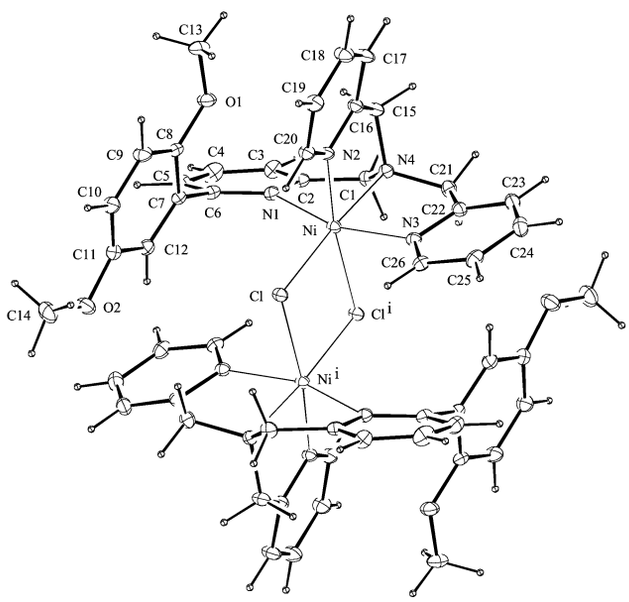

Fig. 4 View of the $[Ni_2Cl_2(L)_2]^{2+}$ ion showing the 10% thermal ellipsoids at 294 K.

co-ligands. The Ni–Cl bond lengths are 2.356(1) and 2.492(2) Å and the Ni–Cl–Ni bond angle is 95.6(1)°. That the Ni–N_{py*} bond [2.167 Å] is notably longer than the other Ni–N bond lengths [2.056–2.094 Å, Table 1] is directly attributable to the steric interactions introduced by the dimethoxyphenyl substitution of the PY* leg. The bond distances and angles, with the exception of those for the Ni–N_{py*} bond, are similar to those recently reported for the corresponding Ni(tpa) dimer, $[Ni_2(\mu\text{-}Cl)_2(tpa)_2][ClO_4]_2$.[26] Notably, the dimethoxyphenyl rings in $[Ni_2(\mu\text{-}Cl)_2(L)_2]Cl_2$ are near parallel to the $Ni_2(\mu\text{-}Cl)_2$ plane which requires a large dimethoxyphenyl–pyridyl inter-annular twist of 72°. This arrangement minimises interactions between the dimethoxyphenyl and the pyridyl rings lying in the plane of the $Ni_2(\mu\text{-}Cl)_2$ core and maximises stabilising dimethoxyphenyl edge C–H-to-pyridyl face interactions between PY* and PY legs on adjacent Ni centres (see Fig. 4); the dimethoxyphenyl edge carbon to pyridyl plane

† *Note added at proof*: a report of the ferrous chloride complexes of four tpa derivatives, which includes crystal structures for octahedral $[FeCl_2(\kappa^4N\text{-tpa})]$ and trigonal bipyramidal $[FeCl_2(\kappa^3N\text{-}Ph_2tpa)]$ and data indicating the structure of each complex is conserved in acetonitrile solution, has appeared: D. Mandon, A. Machkour, S. Goetz and R. Welter, *Inorg. Chem.*, 2002, **41**, 5364.

distance is ~3.7 Å. Space-filling models reveal the ligands L in this structure to completely enclose and shield the $Ni_2(\mu\text{-}Cl)_2$ core.

[CuCl(L)][PF$_6$]. As the structures of [CuCl(L)][PF_6] and "$CuCl_2$(L)" in dichloromethane solution differ (see below), crystal structure analyses were completed for both of these Cu(II) complexes. The crystal structure of [CuCl(L)]Cl·3H_2O is already described elsewhere.[18] Suitable crystals of [CuCl(L)][PF_6] were obtained by recrystallisation from dichloromethane–methanol. In each cation, the Cu(II) ion is bound by the four nitrogens of L and by a chloride ancillary ligand in a slightly distorted square pyramidal arrangement ($\tau = 0.15$). The two N_{py} and the N_{am} donors of L and the ancillary chloride form the basal plane of the pyramid, and the bulkier PY* leg adopts the axial position with the Cu–N distance of 2.509(3) Å being substantially longer than the Cu–N_{am} [2.051(3) Å] and equatorial Cu–N_{py} (av. 1.98 Å) distances. The average N_{am}–Cu–N_{py} angle is 83.1° and the N_{am}–Cu–N_{py*} angle is 80.1(1)° and the interannular twist between the rings of the PY* leg is 24°. In the crystal structure, Fig. 5, cations of [CuCl(L)][PF_6] are arrayed

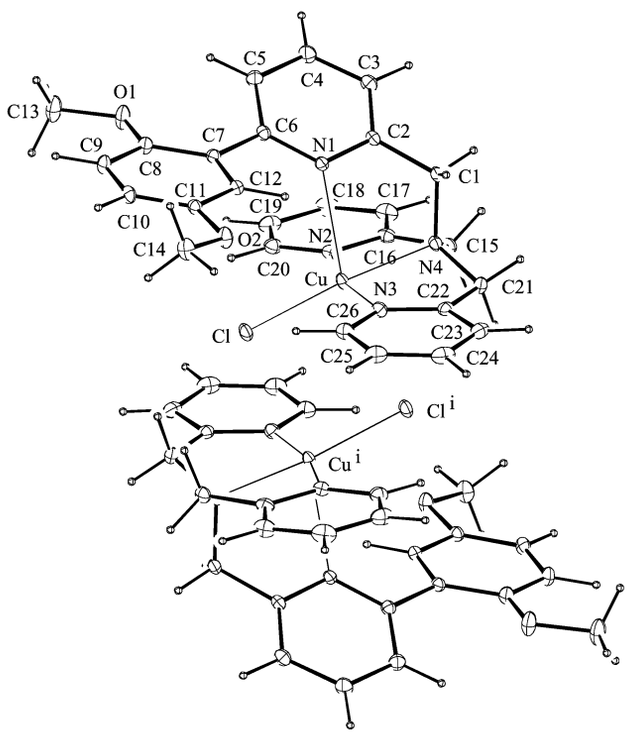

Fig. 5 View of a symmetry-related pair of $[CuCl(L)]^+$ ions (10% thermal ellipsoids at 294 K); the Cu···Cl^i distance is 3.5 Å.

in centrosymmetric pairs with the chloride of one occupying the sixth "octahedral" position of the other; overall the structure of the pair is akin to that of the Ni(II) dimer, but the inter-cation Cu···Cl^i distance is 3.5 Å more consistent with description as a pair of cations. Also of note is the different positioning of the PY* legs in the Ni(II) and Cu(II) complexes revealed by a comparison of Figs. 4 and 5. The structure of the Cu(II) cation is very similar to those of the two crystallographically independent, square pyramidal cations (cation A: $\tau = 0.03$; cation B: $\tau = 0.003$) within the structure of [CuCl(L)]Cl·3H_2O in which there are no inter-cation Cu···Cl interactions.[18] In contrast, [Cu(tpa)Cl][PF_6] adopts a trigonal bipyramidal coordination geometry ($\tau = 1.005$) with the amine group and the chloride co-ligand in the axial positions and with the three pyridyl rings equatorial.[10] Adoption of the square pyramidal geometry by the $[CuCl(L)]^+$ cation minimises intramolecular steric interactions with the bulky PY* leg.

[{Cu(L)}$_4$(CO$_3$)$_2$][BF$_4$]$_4$·5.2H$_2$O. Green crystals of the bis(carbonato)-bridged tetramer, [{Cu(κ^3*N*-L)}$_2${Cu(κ^4*N*-L)}$_2${μ_3-(η^1-*O*,η^2-*O*′)-CO_3}$_2$][BF_4]$_4$·5.2H_2O crystallised from acetonitrile–ether. The identity and structure of the complex was established by X-ray crystallography, Fig. 6 and Table 2. The tetramer is centrosymmetric with each of the four Cu(II) ions best described as five-coordinate and close to square-pyramidal in geometry. The outermost pair of copper ions, $(CuB)_2$, each have a N_4O-donor set: L is tetradentate with the bulky PY* leg in the weak-field, axial position (CuB–N_{py}* 2.25 Å) and with a carbonato oxygen (O2C) and the N_{am} and two N_{py} nitrogens equatorially bound at usual distances (CuB–$N_{am/py}$ ~ 2.0 Å). A second carbonato oxygen (O1C) bridges the innermost pair of copper ions, $(CuA)_2$, each of which shows N_3O_2-donor set with the PY* leg unbound and dangling away from the $Cu_4(\mu\text{-}CO_3)_2$ core. Equatorially bound to each CuA ion at normal distances are O1C of one carbonato ligand, and the N_{am} and two N_{py} nitrogen atoms. The bridging oxygen atom of the other carbonato ligand takes up the axial position (CuA–O1C^i 2.41 Å). The third oxygen atom of each carbonato ligand (O3C) lies between a CuA–CuB pair and could be considered a second axial ligand to these copper ions, albeit weakly bound given the distances (CuA···O3C 2.62, CuB···O3C 2.62 Å). Each of the latter carbonato oxygen atoms is also hydrogen bonded with a water molecule (O3C···OW1 2.77 Å). The Cu_4{μ_3-(η^1-*O*,η^2-*O*′)-CO_3}$_2$ core is not unique, having been recently discovered in a copper(II) carbonato complex of a tetrapyrazolyldiamine macrocycle.[27] In contrast, (tpa)Cu^{II} forms a very different carbonato complex, [{Cu(κ^4*N*-tpa)}$_2${μ_2-(η^1-*O*,η^1-*O*′)-CO_3}]$^{2+}$, which has a single symmetrical, bridging-bidentate carbonato ligand equatorially bound to two square pyramidal copper(II) ions.[28]

Table 2 Selected key bond length (Å) and bond angle (°) data for [Cu_4(L)$_2$(CO_3)$_2$][BF_4]$_4$·5.2H_2O

CuA–N2A	1.982(5)	CuB–N1B	2.251(6)
CuA–N3A	1.974(5)	CuB–N2B	1.954(5)
CuA–N4A	2.017(7)	CuB–N3B	1.973(5)
CuA–O1C	1.957(6)	CuB–N4B	2.057(7)
CuA–O1C^i	2.411(6)	CuB–O2C	1.948(5)
N2A–CuA–N3A	164.2(3)	N1B–CuB–N2B	87.0(2)
N2A–CuA–N4A	82.8(3)	N1B–CuB–N3B	101.7(2)
N2A–CuA–O1C	98.5(3)	N1B–CuB–N4B	81.6(3)
N2A–CuA–O1C^i	97.3(2)	N1B–CuB–O2C	123.1(3)
N3A–CuA–N4A	82.4(3)	N2B–CuB–N3B	162.9(3)
N3A–CuA–O1C	96.8(3)	N2B–CuB–N4B	84.2(3)
N3A–CuA–O1C^i	89.0(2)	N2B–CuB–O2C	94.3(3)
N4A–CuA–O1C	172.8(3)	N3B–CuB–N4B	82.7(3)
N4A–CuA–O1C^i	92.7(2)	N3B–CuB–O2C	93.1(3)
O1C–CuA–O1C^i	80.2(3)	N4B–CuB–O2C	155.2(3)

[$ZnCl_2$(L)]. Colourless rhombs of [$ZnCl_2$(L)] crystallised from methanol–ether. The crystal structure reveals chains of [$ZnCl_2$(L)] molecules, weakly linked by edge-to-face intermolecular interactions between a pyridyl ring of each molecule of [$ZnCl_2$(L)] and the dimethoxyphenyl ring of an adjacent molecule; the edge carbon to adjacent ring plane distances are ~3.5 Å. Each chain has a partner chain running in the opposite direction, with pairs of complex molecules in adjacent chains related by crystallographic inversion. In [$ZnCl_2$(L)] molecules, Fig. 7, the Zn(II) ion exhibits a trigonally-distorted square pyramidal coordination geometry ($\tau = 0.29$) with the base comprised of Cl2 and N_{am} and the two N_{py} donors of L and with Cl1 at the apex. The Zn–Cl bond lengths for the equatorial and axial chlorides are similar [Zn–Cl1 2.234(1) Å; Zn–Cl2 2.244(1) Å]. The PY* leg is unbound, 'dangling' away from the metal centre; the interannular twist between the pyridine and dimethoxyphenyl rings is 50°. In contrast, all crystallographically characterised (tpa)zinc complexes exhibit tetradentate tpa ligands: *e.g.*, [ZnX(tpa)][ClO_4] (X = Cl, Br),[23] [Zn_2(tpa)$_2$(μ-OH)$_2$](ClO_4)$_2$ and [Zn_3(tpa)$_3$(μ-CO_3)](ClO_4)$_4$·H_2O,[29] and [ZnX(tpa)][BPh_4] (X = Cl, $PhCO_2$).[30]

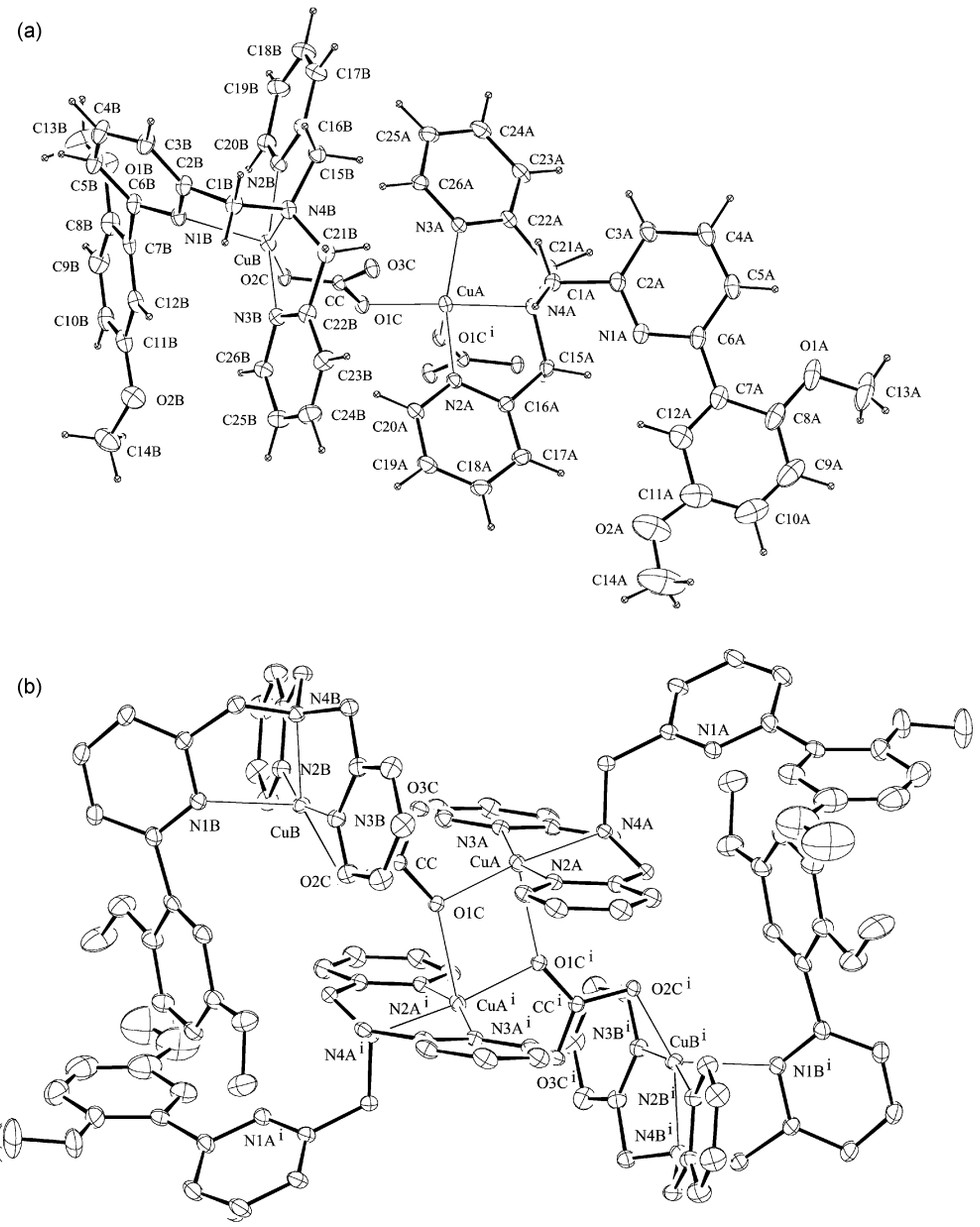

Fig. 6 Views of the $[Cu_4(L)_4(CO_3)_2]^{4+}$ ion (10% thermal ellipsoids) showing: (a) the asymmetric unit and (b) the full tetramer (with H-atoms omitted for clarity).

Solid-state measurements

Bulk samples of all complexes except $[Cu_4(L)_4(CO_3)_2][BF_4]_4$ gave correct partial elemental analyses; $[Cu_4(L)_4(CO_3)_2][BF_4]_4$ was not analysed due to lack of sample. FTIR spectra of the bulk samples show characteristic pyridine-ring deformation bands,[31] Table 3, which indicate ligand coordination modes in accord with the crystal structure analyses. The Mn(II), Fe(II), Co(II), Ni(II) and Cu(II) complexes are paramagnetic and magnetic moments of the bulk samples were obtained by Gouy balance measurements, Table 3. The magnetic moment of the Ni(II) complex is consistent with ferromagnetically coupled Ni centres within the dimeric cations,[32] those of the Cu(II) complexes are as expected, and those of the Mn(II), Fe(II) and Co(II) complexes are indicative for high-spin species, all in keeping with the deductions from the crystal structures.

Table 3 Magnetic moment data at 295 K from Gouy balance measurements and pyridine-ring deformation band data from FTIR spectra along with the indicated number of bound *N*-donors

	$\nu_{py\ +\ py^a}$/cm^{-1}	No. bound N	μ/μ_B
$[MnCl_2(L)]$	1602, 1572	4	5.94
$[FeCl_2(L)]$	1601, 1571	4	5.32
$[CoCl(L)]_2[CoCl_4]$	1607, 1568	4	[a]
$[CoCl(L)][BPh_4]$	1608, 1572	4	4.70
$[Ni_2Cl_2(L)_2]Cl_2$	1605, 1567	4	3.21
$[CuCl(L)]Cl$	1608, 1573	4	1.93
$[CuCl(L)][PF_6]$	1609, 1581	4	1.96
$[ZnCl_2(L)]$	1605, 1585, 1572	3	[a]

[a] Not measured.

Solution-state measurements

Electrospray ionisation mass spectra. Table 4 presents results from positive-ion ESI-MS spectra for the complexes which were introduced into the spectrometer using 1% acetic acid in 1 : 1 aqueous acetonitrile as the feed solvent. Strong peaks for the molecular ion were observed for $[CuCl(L)]^+$, $[CoCl(L)]^+$ and $[Ni_2Cl_2(L)_2]^{2+}$, along with peaks for the ions $[M(L)]^{2+}$ and $[M(L) + OAc]^+$ which arise from chloride dissociation and chloride–acetate exhange,[23] respectively. In contrast, the positive-ion ESI-MS spectra of $[MCl_2(L)]$ (M = Mn, Fe and Zn)

Table 4 Major ions (*m*/*z*) observed by positive-ion electrospray ionisation mass spectroscopy[a]

	$[MCl_2(L) + H]^+$	$[M(L)(OAc)]^+$	$[MCl(L)]_n^{n+}$	$[M(L)]^{2+}$	Other ions
$[MnCl_2(L)]$	553 (1)	540 (8)	517 (3)	241 (1)	427[c] (100)
$[FeCl_2(L)]$	571[b] (10)	541 (100)	517 (22)	241 (52)	
$[CoCl(L)]_2[CoCl_4]$		544 (38)	520 (100)	243 (70)	311 (65)
$[CoCl(L)][BPh_4]$			520 (75)	243 (100)	
$[Ni_2(\mu\text{-}Cl_2)(L)_2]Cl_2$		543 (10)	519 (30)	242 (100)	263 (15)
[CuCl(L)]Cl		548 (42)	526 (100)	245 (10)	
$[CuCl(L)][PF_6]$			524 (100)	245 (60)	
$[ZnCl_2(L)]$	562 (5)				427[c] (100)

[a] Relative peak heights (%) are indicated in parentheses. Only the most intense peak for each ion is quoted; the correct isotope pattern for each ion was observed. The feed solvent employed was 1% acetic acid in 1 : 1 water–acetonitrile. [b] Peak for $[FeCl_2(L) + H_3O]^+$. [c] Peak for $[HL]^+$.

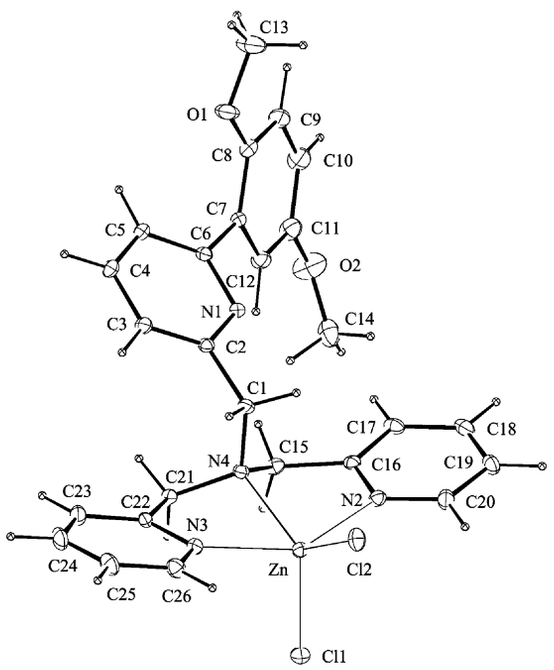

Fig. 7 View of $[ZnCl_2(L)]$ showing the 10% thermal ellipsoids at 294 K.

were much harder to obtain, requiring higher receiver plate gains and higher cone voltages, and are dominated by peaks for $[M(L) + OAc]^+$ and HL^+ along with weaker peaks for $[MCl_2(L) + H]^+$ from protonation of the complex. The results indicates the Co, Ni and Cu complexes to dissolve as ions in the polar acetonitrile–water solution, whereas the Mn, Fe, Zn complexes do not thus requiring fragmentation or exchange of two chlorides for acetate to produce ions.

Electrical conductivity. Table 5 presents salient data from measurements on dilute (~1 mM) solutions of the complexes in dichloromethane. The dichloride complexes are all non-electrolytes, $[MCl_2(L)]$, which is noteworthy for the Ni(II) and Cu(II) complexes since the crystal structures of these show discrete $[Ni_2(\mu\text{-}Cl)_2(L)_2]^{2+}$ or $[CuCl(L)]^+$ cations, respectively, and chloride anions.

Electronic spectra. Data for the ligand and the complexes recorded in dichloromethane solution are presented in Table 6. Two intense ligand-centred bands at 38 900–37 600 and 31 750–30 600 cm^{-1} are found in all electronic spectra, and are the only peaks (with extinction coefficients >1 $dm^3\ mol^{-1}\ cm^{-1}$) observed for the Mn(II) and Zn(II) complexes, consistent with the high-spin d^5 and the d^{10} electron configurations, respectively. The visible–NIR bands of the other metal complexes, Fig. 8, are assigned to d–d transitions and give information about the stereochemistry in solution. For $[FeCl_2(L)]$, the weak band at 8 810 cm^{-1} is assigned to the $^5E_g \longleftarrow {}^5T_{2g}$ transition (at

Table 5 Molar electrical conductivity values (± 10%) for the complexes (~1 mM) in dichloromethane

	Λ_M/S $cm^2\ mol^{-1}$
$[MnCl_2(L)]$	2.9
$[FeCl_2(L)]$	4.1
$[CoCl(L)][BPh_4]$	21.1
$[NiCl_2(L)]$	3.6
$[CuCl_2(L)]$	4.5
$[CuCl(L)][PF_6]$	24.1
$[ZnCl_2(L)]$	3.8
$[NBu_4][PF_6]$	26.3

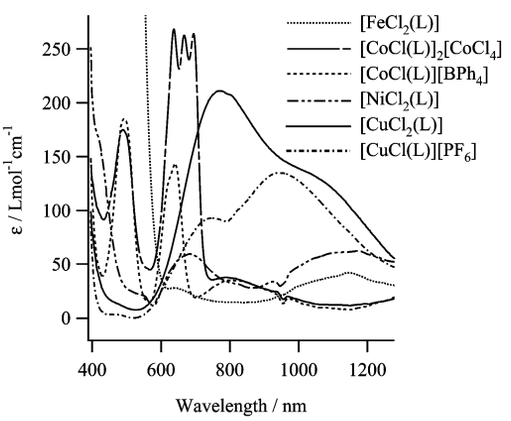

Fig. 8 Vis-NIR spectra for the metal(II) chloride complexes of L in dichloromethane.

an energy of 10*Dq*), which is the only spin-allowed transition for the high-spin octahedral d^6 Fe^{2+} ion.[34] The electronic spectra of $[CoCl(L)][BPh_4]$ and $[CoCl(L)]_2[CoCl_4]$ are comparable to those of the prototypal trigonal-bipyramidal Co(II) complexes $[CoBr(Me_3tren)]Br$ and $[CoCl(tren)]Cl$.[34–36] The spectrum of $[CoCl(L)][BPh_4]$ displays peaks at 20 410 cm^{-1}, 15 625 cm^{-1} and a shoulder at 12 225 cm^{-1} attributable to the characteristic $^4E''(P) \longleftarrow {}^4A'_2(F)$, $^4A'_2(P) \longleftarrow {}^4A'_2(F)$ and $^4E''(F) \longleftarrow {}^4A'_2(F)$ transitions, respectively, of a high-spin *tbp*-d^7 Co(II) complex.[34–36] The spectrum of $[CoCl(L)]_2[CoCl_4]$ shows these d–d bands overlaid with the diagnostic peaks at 15 015–14 370 cm^{-1} for the $^4T_1(P) \longleftarrow {}^4A_2$ transition of the $[CoCl_4]^{2-}$ anion. The electronic spectrum of the Ni(II) complex in dichloromethane, $[Ni(L)Cl_2]$, shows three d–d bands at 8 550 cm^{-1} (ν_1), 14 665 cm^{-1} (ν_2) and 23 800 cm^{-1} (ν_3—this band appears as a shoulder to a higher energy ligand-centred transition). The spectrum is diagnostic for a five-coordinate complex species having a N_3Cl_2 donor set.[31,32,37] The electronic spectrum of $[CuCl(L)][PF_6]$ exhibits a peak at 10 750 cm^{-1} with a higher energy shoulder at 13 700 cm^{-1}, a pattern indicative for a five-coordinate copper(II) centre with trigonal pyramidal geometry.[10,11,18,38] Likewise the X-band EPR spectrum in dichloromethane at 77 K shows an 'inverse' axial pattern with $g_\perp = 2.235$ ($A_\perp = 112$ G) and $g_{||} \approx 2.0$ ($A_{||} \approx 86$ G), characteristic

Table 6 Electronic absorption spectral data for the complexes in dichloromethane solution

	λ_{max}/nm (ε/dm^3 mol^{-1} cm^{-1})
L	260 (14 250), 318 (7040)
$[MnCl_2(L)]$	265 (7650), 328 (4900)
$[FeCl_2(L)]$	261 (10 000), 327 (5100), 421 (950), 1135 (25)
$[CoCl(L)][BPh_4]$	263 (14 000), 327 (3380), 490 (190), 621 (130), 640 (150), 818 (35)
$[CoCl(L)]_2[CoCl_4]$	266 (9600), 325 (3150), 488 (175), 635 (270), 666 (270), 696 (270), 805 (36)
$[NiCl_2(L)]$	262 (10 350), 326 (3500), 420 (180), 682 (65), 1170 (68)
$[CuCl_2(L)]$	257 (17 700), 320 (8000), 770 (200), 1050 (130)
$[CuCl(L)][PF_6]$	265 (13 800), 315 (5050), 730 (106), 930 (130)
$[ZnCl_2(L)]$	267 (9650), 325 (3200)

for a trigonal bipyramidal species with a d_{z^2} ground-state. In contrast, $[CuCl_2(L)]$ displays a peak at 12 990 cm^{-1} with a lower energy shoulder at 9 525 cm^{-1} and the X-band EPR spectrum is axial with $g_{||}$ = 2.236 ($A_{||}$ = 176 G) and $g_{\perp}$ = 2.027, data all consistent with a square pyramidal Cu(II) species.[10,11,18,38]

Variable-temperature ^{1}H NMR spectroscopy. Of the complexes, only $[ZnCl_2(L)]$ is diamagnetic. In the ambient temperature spectrum the peak for the diastereotopic methylene protons was noticeably broad and therefore a variable-temperature ^{1}H NMR study was undertaken, Fig. 9. In the

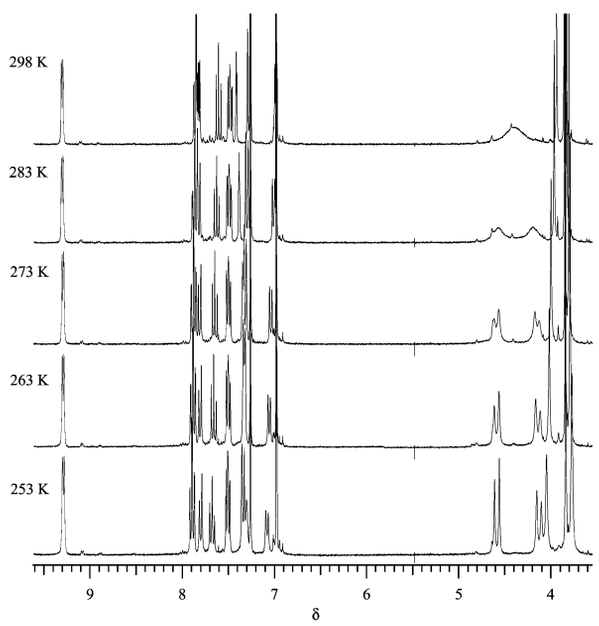

Fig. 9 Variable-temperature 300 MHz ^{1}H-NMR spectra for $[ZnCl_2(L)]$ in $CDCl_3$.

298 K spectrum, an exchange-broadened singlet is observed at δ_H 4.40 for the diastereotopic methylene protons. As the temperature is lowered, the broad methylene peak coalesces and then emerges as a pair of AB doublets at δ_H 4.61 and 4.15, which sharpen in the lower temperature spectra. The coalescence temperature (T_c) is 290 ± 3 K, which corresponds to a free energy barrier ($\Delta G^{\ddagger}_{290\ K}$) of 56 ± 0.5 kJ mol^{-1} for exchange of the diastereotopic methylene protons.[39] The pyridyl and aryl proton peaks remain sharp in all spectra and are consistent with an unbound PY* and two bound PY legs for the complex in solution. Separate sets of peaks for L and the complex were observed when excess free L was deliberately added, implicating an intramolecular fluxional process in the exchange of the diastereotopic methylene protons in the complex. This must involve pyramidal inversion of the amine, which is typically a low energy process[40,41] but for $[ZnCl_2(L)]$ requires *at a minimum*

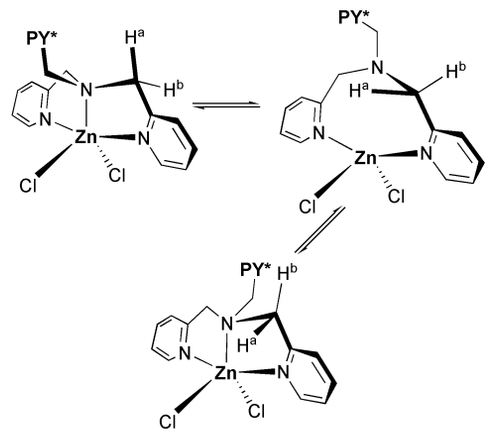

Scheme 1 A possible mechanism for exchange of the diastereotopic methylene protons in the $[ZnCl_2(L)]$.

dissociation of one pyridyl leg and the amine from the zinc ion. Scheme 1 depicts a possible mechanism. The energy barrier for pyramidal inversion of dibenzylmethylamine is 28 ± 3 kJ mol^{-1},[41] which provides an estimate for the lower limit to the barrier for inversion in L, considerably smaller than that for $[ZnCl_2(L)]$ and consistent with complex formation constraining the pyramidal inversion of the amine.

Discussion

Solid-state structures

The crystal structures presented here are the most complete set of first d-series metal(II) halide complexes for a particular "tpa-like" ligand. Fig. 10 diagrammatically presents the key

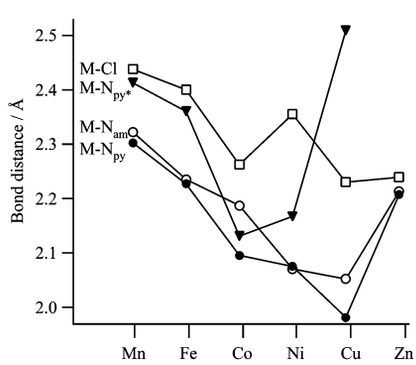

Fig. 10 Plot showing a comparison of the metal-to-ligand bond distances in the metal(II) chloride complexes of L (the average M–Cl and M–N_{py} distance is indicated).

metal-to-ligand bond length data for these $[M^{II}Cl_x(L)]^{(2-x)+}$ (x = 1, 2) complexes. For the Mn^{2+}–Co^{2+} complexes, where high- or low-spin d^n-electron configurations are possible, the metal-to-ligand bond distances are all indicative for a high-spin

Table 7 Coordination properties of the divalent metal–chloride complexes of L

	Mn^{2+}	Fe^{2+}	Co^{2+}	Ni^{2+}	Cu^{2+}	Zn^{2+}
Coordination number	6	6	5	6	5	5
Coordination sphere	N_4Cl_2	N_4Cl_2	N_4Cl	N_4Cl_2	N_4Cl	N_3Cl_2
Stereochemistry	O_h [a]	O_h [a]	*tbp* [b]	O_h [a]	*sp* [c]	*d-sp* [d]
Metal ion radius [e]/Å	0.97	0.92	0.89 (0.81)	0.83 (0.77)	0.87 (0.79)	0.88 (0.82)

[a] Octahedral. [b] Trigonal bipyramidal. [c] Square pyramidal. [d] Trigonally-distorted square pyramidal. [e] Values for high-spin six-coordinate (and high-spin five-coordinate) metal ions taken from ref. 43.

Table 8 Ligand field stabilisation energies (in *Dq*) for ideal five- and six-coordinate complexes

	Square pyramidal [a]		Trigonal bipyramidal [a]		Octahedral	
	Strong-field	Weak-field	Strong-field	Weak-field	Strong-field	Weak-field
Co^{2+} (d^7)	−19.14	−9.14	−13.34	−5.45	−18.0	−8.0
Ni^{2+} (d^8)	−18.28	−10.00	−14.16	−6.27	−12.0	
Cu^{2+} (d^9)	−9.14		−7.09		−6.0	

[a] Pyramid base in the *xy* plane.

complex, which is anticipated given the π-donor chloride ancillary ligands and the weakening of the ligand field caused by the steric interactions introduced by the dimethoxyphenyl substitution of the PY* leg (which in all cases is the more weakly bound leg). The general trend of decreasing metal-to-ligand bond lengths from Mn^{2+} to Cu^{2+} tracks the increasing effective nuclear charge. The apparent "dip" in the metal-to-ligand bond lengths for the Co(II) complex compared to its Fe(II) and Ni(II) neighbours simply reflects the dependence of the metal ionic radius upon coordination number: the Co(II) complex is five-coordinate whereas its neighbours are six-coordinate, Table 7. Similarly the six-coordinate Ni(II) complex is flanked by five-coordinate Co(II) and Cu(II) neighbours. Ligand-field arguments suffice to rationalise the other deviations from the general decline in metal-to-ligand bond lengths. For example, the marked increase in the $M–N_{py*}$ bond length in the square pyramidal $[CuCl(L)]^+$ ion corresponds to the filling of the d_{z^2} orbital (the static Jahn-Teller effect for the d^9 Cu^{2+} ion). Likewise for the d^{10} Zn(II) complex where the full d-subshell results in the comparatively longer coordination bonds.

Table 7 summarises the coordination geometries and environments found in the crystal structures and lists ionic radii for the high-spin five- and six-coordinate metal ions. Six-coordination is observed for the larger high-spin Mn^{2+} and high-spin Fe^{2+} ions where the ionic radius of the six-coordinate ion is greater than 0.9 Å, whereas five-coordination appears preferred when the metal ion is smaller than this. The exception is the Ni(II) complex — here the d^8 Ni^{2+} ion is in a weak-field environment and, although only a small component of the overall bonding energy, the ligand field stabilisation energy (LFSE: −12 *Dq*) favours the octahedral complex, Table 8. From the LFSE values in Table 8 it appears that the d^7 Co(II) complex should adopt a square pyramidal geometry. However, the listed LFSE values are for ideal geometries with $L_{apical}–Co^{II}–L_{basal}$ angles of 90°, and if the $L_{apical}–Co^{II}–L_{basal}$ angles deviate by 15° from this, as they must for $[CoCl(L)]^+$ due to the constraints imposed by L, a trigonal bipyramidal geometry becomes favoured.[36] Also noteworthy is that only in $[ZnCl_2(L)]$ is the PY* leg dangling, displaced by a second chloride — the larger ligand-field splittings with π-acceptor pyridyl compared to a π-donor chloride ligand favour coordination of the PY* leg for all of the metal ions except the d^{10} Zn(II) ion (LFSE = 0 *Dq*). Finally, although not one of the $[M^{II}Cl_x(L)]^{(2-x)+}$ series, the structure of the $[Cu_4(L)_4(CO_3)_2]^{4+}$ ion suggests the binding of the PY* leg to Cu(II) becomes more finely balanced when the ancillary ligand lies closer to pyridine in the spectrochemical series.

Solution behaviour

The ESI-MS spectral results for the $[M^{II}Cl_x(L)]^{(2-x)+}$ (x = 1, 2) complexes strongly suggest that each gives the same species in polar acetonitrile–water solution as found in its crystal structure (see above). However, in dichloromethane, which has a comparatively low dielectric constant ($\varepsilon_r \approx 8.9$ at 25 °C), separation into ions is less favourable, and the molar conductivity values reveal that a second chloride, when available, coordinates to the metal centres. For the dichloride complexes of the smaller metal ions, the electronic [for Ni(II) and Cu(II)], EPR [for Cu(II)] and NMR [for Zn(II)] spectral data are indicative of five-coordinate $[MCl_2(\kappa^3N\text{-L})]$ structures in dichloromethane solution, consistent with displacement of the bulky and more weakly bound PY* leg by the second chloride ligand. In contrast, $[CuCl(\kappa^4N\text{-tpa})]^+$ in dichloromethane is unreactive toward extra chloride ion.[18]

Conclusions

The structures and/or physicochemical properties of the transition metal complexes of L differ considerably from those of their tpa-analogues. A single 6-aryl substituent to the tpa skeleton is sufficient to alter the chemistries of the resulting metal complexes: the intramolecular steric interactions introduced by the single dimethoxyphenyl-substituent prevent N_{py*} from approaching close to a metal centre and, consequently, weaken the ligand field of L compared to tpa thereby favouring high spin complexes. For the smaller metal ions, the steric effect of the dimethoxyphenyl substituent is exacerbated to the point where there is a fine balance between bound and unbound PY* legs — hemilability — in the Ni(II) and Cu(II) systems and no evidence for binding of the PY* leg in the Zn(II) dichloride complex. Moreover, binding of the PY* leg in the Ni(II) and Cu(II) systems can be conveniently modulated by (the availability of) the ancillary ligands and (changes to) the solvent. Comparable hemilability in the Ni(II) and Cu(II) complexes of alkyl-tpa derivatives is found only when the tpa-skeleton has three 6-alkyl substituents. An advantage of mono(6-aryl) substitution of the tpa-skeleton is that the coordinative lability is predicably restricted to the bulkier aryl-substituted leg (PY*) of the Ni(II) and Cu(II) complexes, a useful feature which possibly could be exploited in designs for new molecular devices based upon, for example, pH- or redox-controlled switching of the conformation and binding of the PY* leg.[18,42]

Two final points: First, $[Cu_4(L)_4(CO_3)_2]^{4+}$ is the first complex species to exhibit both κ^3N- and κ^4N-bound tpa-related ligands within the same molecule or ion. Second, the NMR spectra of

$[ZnCl_2(L)]$ exhibit fluxional behaviour attributable to pyramidal inversion of the amine donor of L with $\Delta G^{\ddagger}_{(290\ K)} = 56 \pm 0.5$ kJ mol^{-1}; to our knowledge this is the first time this process has been characterised in a transition metal complex of tpa or a ligand based upon the tpa-skeleton.

Experimental

Elemental analyses for C, H and N were determined by the Australian National University Microanalytical Unit. Electrospray mass spectra (ESI-MS) were acquired on a VG Quattro mass spectrometer employing capillary voltages of 3–5 kV and cone voltages of 5–60 V. The solvent system was 50 : 50 acetonitrile–water, depending on the sample, with or without 1% acetic acid added. ^1H and $^{13}C\{^1H\}$ NMR spectra were recorded on a Bruker AC 300F (300 MHz) spectrometer. Electronic spectra of solutions of the complexes in 1 cm quartz cuvettes were recorded between 240 and 2000 nm on a CARY 5 spectrometer in the dual beam mode. The solutions of $[FeCl_2(L)]$ were prepared under nitrogen in a M. Braun glovebox. X-Band EPR spectra of both frozen solution (at 77 K; liquid nitrogen dewar) were recorded using a Bruker EMX 10 EPR spectrometer. Electrical molar conductivity measurements were made using an in-house built conductivity bridge and a YSI model 3403 conductivity cell thermostated at 25 °C. The cell constant (K) was determined with a standard aqueous solution of KCl (0.001 M). The molar conductivity, Λ_M, of a sample solution was determined from $\Lambda_M = 1000K/c_m$, where c_m is the molar concentration of the complex (*ca.* 1 mM).

Preparation of [6-(2′,5′-dimethoxyphenyl)-2-pyridylmethyl)]-bis(2-pyridylmethyl)amine (L)

I. Precursors. *2,5-Dimethoxyphenylboronic acid.* *n*-Butyllithium [14.5 mL (2.5 M in hexane), 36 mmol] was added to 1,4-dimethoxybenzene (5.4 g, 36 mmol) in anhydrous diethyl ether (100 mL). After 2 h the mixture was added dropwise to a solution of tri(*iso*-propyl)borate (16.9 mL, 72 mmol) in dry diethyl ether (10 mL) cooled to −70 °C. After addition, the mixture was stirred for 30 min at −70 °C, then warmed to ambient temperature and stirred for 16 h. Diethyl ether (100 mL) and 10% aqueous HCl (100 mL) were added and the organic layer separated, washed with water (40 mL) and dried over magnesium sulfate. The solvent was removed and the product(s) separated by flash chromatography on silica (hexane–dichloromethane 3 : 1 eluent). The second major fraction was collected and recrystallisation from hexane–dichloromethane gave a white crystalline solid (4.6 g, 72%), mp 91–93 °C (Found: C, 52.38; H, 6.22. $BC_8H_{11}O_4$ requires C, 52.80; H, 6.09%); *m*/*z* (EI-MS) 182 (M^+); δ_H ($CDCl_3$) 7.38 (1H, br d, Ph), 6.97 (1H, dd, Ph), 6.86 (1H, d, Ph), 5.89 (2H, s, OH), 3.88 (3H, s, CH_3O), 3.81 (3H, s, CH_3O).

6-Bromo-2-pyridylcarboxyaldehyde. The method of Chuang *et al.*[14] was adapted as follows. To a slurry of 2,6-dibromopyridine (19.0 g, 0.08 mol) in anhydrous diethyl ether (150 mL), cooled to below −60 °C using an acetone-slush cooling bath, *n*-butyllithium [32 mL (2.5 M in hexane), 0.08 mol] was added at a rate such that the temperature did not exceed −60 °C. After addition was complete, the reaction mixture was allowed to warm to −40 °C for 15 min; a clear yellow solution resulted. This solution was cooled to −80 °C and a solution of dimethylformamide (6.4 g, 0.088 mol) in dry diethyl ether (10 mL) was added keeping the temperature below −70 °C. Stirring was continued for 2 h at this temperature, producing a grey precipitate. The mixture was then allowed to warm to −10 °C and hydrolysed with 6 M hydrochloric acid (30 mL). The aqueous phase was separated and extracted with diethyl ether. The extracts and the original diethyl ether phase were combined, washed with water, dried over magnesium sulfate and concentrated by rotary evaporation until crystallisation commenced. The product was collected by filtration. Additional product was obtained by further concentration of the mother liquor and addition of *n*-pentane to give 11.1 g (75%) of the product as white flakes, mp 80–81.5 °C; *m*/*z* (EI-MS) 186 (M^+, 90%), 158 (50), 78 (100); δ_H ($CDCl_3$) 9.93 (s, 1H, CHO), 7.60–7.92 (3H, m, Py).

*6-(2′,5′-Dimethoxyphenyl)-2-pyridylcarboxyaldehyde (**A**).* 6-Bromo-2-pyridylcarboxyaldehyde (1.67 g, 9.0 mmol) and $Pd(PPh_3)_4$ (0.50 g, 0.43 mmol) were dissolved in toluene (40 mL) under a nitrogen atmosphere. Aqueous sodium carbonate solution (6 mL, 2 M) and 2,5-dimethoxyphenylboronic acid (1.86 g, 10 mmol) in methanol (10 mL) were added and the solution heated at reflux for 8 h. After cooling, dichloromethane (50 mL), an aqueous sodium carbonate solution (15 mL, 2 M) and concentrated ammonia (2 mL) were added. The solution was extracted with dichloromethane, the organic layer separated and dried over magnesium sulfate and the solvent removed *in vacuo*. The residue was separated by flash chromatography on silica (dichloromethane–toluene 5 : 1 eluent). The second fraction was collected and recrystallisation from dichloromethane–hexane gave a white crystalline solid (1.80 g, 82%), mp 55–56 °C; *m*/*z* (EI-MS) 243 (M^+, 95%), 225 (100), 210 (75), 197 (70); δ_H ($CDCl_3$) 10.16 (s, 1H, CHO), 8.12 (1H, dd, Py), 7.89 (2H, m, Py), 7.52 (1H, s, Ph), 6.98 (2H, m, Ph), 3.86 (3H, s, CH_3O), 3.83 (3H, s, CH_3O); δ_C ($CDCl_3$) 194.57, 156.87, 154.58, 153.11, 152.00, 137.18, 129.97, 129.00, 120.07, 116.64, 116.52, 113.65, 56.87, 56.40; ν/cm^{-1} (KBr disc) 2954w, 2828w, 1708s, 1584s, 1506s, 1463s, 1411s, 1353m, 1288m, 1257s, 1223s, 1185s.

6-(2′,5′-Dimethoxyphenyl)-2-pyridylmethanol. 6-(2′,5′-Dimethoxyphenyl)-2-pyridylcarboxaldehyde (0.20 g, 0.82 mmol) and sodium borohydride (0.04 g, 1.1 mmol) were heated at reflux in methanol (20 mL) for 15 min. The solvent was removed *in vacuo*, water (10 mL) and 1 M sodium hydroxide (3 drops) were added and the reaction mixture extracted with dichloromethane. Removal of the solvent *in vacuo* gave a colourless oil (0.19 g, 95%). *m*/*z* (EI-MS) 245 (M^+); δ_H [$(CD_3)_2$-SO] 7.84 (1H, t, Py), 7.74 (1H, d, Py), 7.43 (1H, d, Py), 7.36 (1H, d, Ph), 7.12 (1H, d, Py), 7.00 (1H, dd, Ph), 5.45 (1H, t, OH), 4.65 (2H, d, CH_2), 3.81 (3H, s, CH_3O), 3.79 (3H, s, CH_3O).

*6-(2′,5′-Dimethoxyphenyl)-2-pyridylmethylbromide (**B**).* 6-(2′,5′-Dimethoxyphenyl)-2-pyridylmethanol (0.66 g, 2.69 mmol) was dissolved in dichloromethane (50 mL), excess phosphorous tribromide (3 mL) added dropwise and the solution stirred for 3 h at room temperature (during this time a white precipitate formed) and then heated at reflux for 30 min. After cooling, the mixture was washed with brine (50 mL), extracted into dichloromethane, dried over magnesium sulfate and the solvent removed *in vacuo*. Recrystallisation from diethyl ether afforded a white crystalline solid (0.65 g, 78%), mp 104–105°C; *m*/*z* (EI-MS) 307 (M^+, 10%), 278 (5), 228 (100), 198 (35); δ_H ($CDCl_3$) 7.77 (1H, d, Py), 7.72 (1H, t, Py), 7.41 (1H, d, Ph), 7.39 (1H, s, Py), 6.93 (2H, m, Ph), 4.63 (2H, s, CH_2), 3.84 (3H, s, CH_3O), 3.81 (3H, s, CH_3O).

II. Method 1. 6-(2′,5′-Dimethoxyphenyl)-2-pyridylmethylbromide (0.9 g, 3 mmol), bis(2-pyridylmethyl)amine (0.7 g, 3 mmol) and triethylamine (5 mmol) were stirred in tetrahydrofuran (50 mL) at ambient temperature for 5 d. The solvent was removed *in vacuo* and the product separated by flash chromatography on silica. Initially, dichloromethane was used as the eluent to remove unreacted 6-(2′,5′-dimethoxyphenyl)-2-pyridylmethylbromide. Then a 95 : 5 dichloromethane–methanol mixture was used to elute a yellow band. This band was collected and the solvent removed to leave a yellow oil which solidified upon drying *in vacuo* to give a cream powder (0.95 g, 74%), mp 128–129 °C (Found: C, 71.96; H, 6.12; N, 12.93. $C_{26}H_{26}N_4O_2 \cdot 0.5H_2O$ requires C, 71.70; H, 6.25; N, 12.86%); *m*/*z* (EI-MS) 426 (M^+); λ_{max}/nm (CH_2Cl_2) 260 (ε/dm^3 mol^{-1} cm^{-1} 14 250), 318 (7040); δ_H ($CDCl_3$) 8.53 (2H, d, Py),

7.70 (6H, m, Py), 7.51 (1H, d, Py), 7.41 (1H, d, Ph), 7.13 (2H, q, Py), 6.99 (2H, m, Ph), 3.96 (2H, s, CH_2), 3.94 (4H, s, CH_2), 3.81 (3H, s, CH_3O), 3.78 (3H, s, CH_3O).

III. Method 2. Sodium cyanoborohydride (0.40 g, 6.35 mmol) was added slowly to an ice-bath cooled mixture of 6-(2′,5′-dimethoxyphenyl)-2-pyridylcarboxaldehyde (1.85 g, 7.5 mmol), bis(2-pyridylmethyl)amine (1.33 g, 6.75 mmol) and acetic acid (0.9 g, 15 mmol) in methanol (50 mL). The resulting solution was stirred at room temperature for 3 d, then acidified by addition of concentrated hydrochloric acid to quench the excess sodium cyanoborohydride. The mixture was evaporated under reduced pressure until almost dry, then water was added and the resulting solution made alkaline by addition of solid sodium carbonate. A dark brown oil separated and was extracted with dichloromethane. The extracts were dried over sodium sulfate and the solvent removed *in vacuo* to afford a brownish oily product (2.7 g, ~100%). Recrystallisation from petroleum ether (bp 60–80 °C)–dichloromethane yielded a white solid (1.96 g, 73%), mp 128–130 °C. The ^{1}H NMR spectral data were identical to those of the ligand prepared by method 1.

Preparation of metal complexes

[$MnCl_2$(L)]. L (102 mg, 0.24 mmol) and $MnCl_2·4H_2O$ (40 mg, 0.2 mmol) were dissolved in methanol (3 mL) and stirred for 10 min. Diethyl ether (15 mL) was added to the solution. A white solid formed which was collected by filtration and washed with diethyl ether. The solid was recrystallised from methanol–diethyl ether (90 mg, 75%), mp 180 °C (decomp.) (Found: C, 55.49; H, 5.11; N, 9.59. $C_{26}H_{26}Cl_2MnN_4O_2·CH_3OH$ requires C, 55.48; H, 5.18; N, 9.59%).

[$FeCl_2$(L)]. Under a nitrogen atmosphere in a Schlenk flask, L (100 mg, 0.235 mmol) and $FeCl_2·6H_2O$ (29 mg, 0.23 mmol) were dissolved in deoxygenated methanol (3 mL). The Schlenk flask was connected to a second containing deoxygenated diethyl ether (20 mL) and set aside. After 2 d, clear yellow crystals of the product had formed and were collected in a nitrogen-filled glovebox (60 mg, 46%), mp 165 °C (decomp.) (Found: C, 55.35; H, 4.91; N, 9.25. $C_{26}H_{26}Cl_2FeN_4O_2·CH_3OH$ requires C, 55.38; H, 5.12; N, 9.57%).

[CoCl(L)]$_2$[$CoCl_4$]. L (102 mg, 0.24 mmol) and $CoCl_2·6H_2O$ (48 mg, 0.2 mmol) were dissolved in methanol (3 mL) and stirred for 15 min. Diethyl ether (15 mL) was added to dilute the solution. The light green powder that formed was filtered off and washed with diethyl ether (80 mg, 72%). This was recrystallised with methanol and diethyl ether to afford a pale green microcrystalline solid (63 mg, 88%), mp 190 °C (decomp.) (Found: C, 49.07; H, 4.50; N, 8.22 $C_{52}H_{52}N_8Cl_6Co_3O_4·2CH_3OH$ requires C 49.46; H 4.73; N, 8.47%).

[CoCl(L)][BPh_4]. Excess Na[BPh_4] (50 mg) in methanol (5 mL) was added to [CoCl(L)]$_2$[$CoCl_4$] (50 mg, 0.04 mmol) in methanol (5 mL). A grey solid precipitated. This was collected by filtration, washed with methanol and then dissolved in dichloromethane (2 mL). Methanol (5 mL) was slowly added and the resulting pale green solution was set aside to slowly evaporate for 3 d. Green hexagonal crystals formed that were suitable for X-ray crystallographic analysis (24 mg, 73%), mp 190 °C (decomp.) (Found: C, 70.25; H, 5.40; N, 6.63. $C_{49}H_{45}N_4BClCoO_2·H_2O$ requires C, 69.98; H, 5.64; N, 6.53%).

[Ni_2Cl_2(L)$_2$]Cl_2. L (102 mg, 0.24 mmol) and $NiCl_2·6H_2O$ (90 mg, 0.2 mmol) were dissolved in methanol (3 mL) and stirred for 10 min. Diethyl ether (15 mL) was added to dilute the solution. A light green microcrystalline solid formed, which was filtered off and washed with diethyl ether (80 mg, 72%). Recrystallisation from a chloroform–heptane–diethyl ether mixture gave crystallographic quality crystals (72 mg, 90%), mp 132 °C (decomp.) (Found: C, 50.82; H, 5.43; N, 8.95. $C_{26}H_{26}Cl_2N_4NiO_2·3H_2O$ requires C, 51.18; H, 5.29; N, 9.18%).

[CuCl(L)]Cl. L (102 mg, 0.24 mmol) and $CuCl_2·2H_2O$ (35 mg, 0.2 mmol) were dissolved in methanol (3 mL). After 10 min diethyl ether (15 mL) was added to dilute the solution. A light blue microcrystalline solid formed which was collected by filtration and washed with diethyl ether. The solid was recrystallised from methanol–diethyl ether (115 mg, 95%), mp 194 °C (decomp.) (Found: C, 55.19; H, 4.64; N, 9.91. $C_{26}H_{26}Cl_2CuN_4O_2$ requires C, 55.67; H, 4.67; N, 9.99%); X-band EPR (CH_2Cl_2, 77 K) $g_{||}$ 2.236 ($A_{||}$ 176 G), $g_{\perp}$ 2.027.

[CuCl(L)][PF_6]. To [Cu(L)Cl]Cl (28 mg, 0.05 mmol) in methanol (5 mL) was added K[PF_6] (9.5 mg, 0.052 mmol) in methanol (5 mL). The pale blue solid which immediately precipitated was collected and recrystallised from dichloromethane–methanol to yield the product, a blue microcrystalline solid (28.4 mg, 85%), mp 238 °C (decomp.) (Found: C, 46.19; H, 3.86; N, 8.30. $C_{26}H_{26}N_4ClCuF_6O_2P$ requires C, 46.58; H, 3.91; N, 8.36%); X-band EPR (CH_2Cl_2, 77 K) $g_{\perp}$ 2.235 ($A_{||}$ 112 G), $g_{||}$ 2.095 ($A_{||}$ 86 G);

[Cu_4(L)$_4$(CO_3)$_2$][BF_4]$_4$. Under nitrogen in a Schlenk flask, L (43 mg, 0.1 mmol) was added to [$Cu(CH_3CN)_4$][BF_4] (32 mg, 0.1 mmol) in deoxygenated acetonitrile (10 mL). A clear yellow solution of [Cu(L)][BF_4][18] formed immediately. The yellow solution was cooled to −40 °C and was bubbled with dry oxygen for 5 min. The solution turned green and was warmed to room temperature. At this point no attempt was made to exclude air from the green solution, a portion of which (4 mL) was layered with diethyl ether (16 mL) and set aside to crystallise. Several green wedge-shaped crystals were obtained after 2 d. The formulation of the compound rests solely on the X-ray crystal structure analysis.

[$ZnCl_2$(L)]. L (46 mg, 0.11 mmol) and $ZnCl_2$ (15 mg, 0.11 mmol) were dissolved in methanol (3 mL). After 10 min diethyl ether (15 mL) was added and the white microcrystalline solid which formed was filtered off and washed with diethyl ether. Recrystallisation from methanol–diethyl ether afforded colourless crystals of the product (50 mg, 81%), mp 226 °C (decomp.) (Found: C, 54.47; H, 4.56; N, 9.77. $C_{26}H_{26}Cl_2N_4O_2Zn·0.5H_2O$ requires C, 54.61; H, 4.76; N, 9.80%); δ_H (300 MHz) ($CDCl_3$, 298 K) 9.30 (dt, 2 H, H^6_{py}), 7.85 (td, 2 H, H^4_{py}), 7.82 (dd, 1 H, $H^{3/5}_{py*}$), 7.61 (d, 1 H, H^4_{py*}), 7.48 (ddd, 2 H, H^5_{py}), 7.42 (td, 1 H, $H^{6'}_{py*}$), 7.28 (dt, 2 H, H^3_{py}), 6.99 (dd, 1 H, $H^{5/3}_{py*}$), 6.98 (m, 2 H, $H^{3',4'}_{py*}$), 4.40 (br s, 4 H, CH_2), 3.94 (s, 2 H, CH_2), 3.86 (s, 3H, CH_3O), 3.84 (s, 3H, CH_3O).

X-Ray crystallography

Relevant crystal and refinement data are collected in Table 9. For [Ni_2(μ-Cl)$_2$(L)$_2$]Cl_2·MeOH·5H_2O one of the lattice chloride counter ions is disordered with the lattice waters. The asymmetric unit contains one half of the dimeric cation (one Ni), and in the lattice half a methanol and half a chloride which are well ordered, along with the disordered half a chloride which was refined distributed over three sites with 2.5 water oxygens.

CCDC reference numbers 190789–190796.

See http://www.rsc.org/suppdata/dt/b2/b207406k/ for crystallographic data in CIF or other electronic format.

Acknowledgements

This research was funded from an UNSW Vice-Chancellor's Goldstar Award.

Table 9 Numerical and refinement data for the X-ray crystal structures

	L	$[MnCl_2(L)]\cdot MeOH$	$[FeCl_2(L)]\cdot MeOH$	$[CoCl(L)][BPh_4]$	$[Ni_2Cl_2(L)_2]Cl_2\cdot MeOH\cdot 5H_2O$	$[CuCl(L)][PF_6]$	$[ZnCl_2(L)]$	$[Cu_4(L)_4(CO_3)_2]\ [BF_4]_4\cdot 5.2H_2O$
Formula (sum)	$C_{26}H_{26}N_4O_2$	$C_{27}H_{30}Cl_2MnN_4O_3$	$C_{27}H_{30}Cl_2FeN_4O_2$	$C_{50}H_{46}BClCoN_4O_2$	$C_{26.5}H_{33}Cl_2N_4NiO_5$	$C_{26}H_{26}ClCuF_6N_4O_2P$	$C_{26}H_{26}Cl_2N_4O_2Zn$	$C_{106}H_{114.4}B_4Cu_4F_{16}N_{16}O_{19.2}$
M	426.5	584.4	585.3	840.1	617.2	670.5	562.8	2521.2
Crystal system	Monoclinic	Orthorhombic	Orthorhombic	Monoclinic	Triclinic	Triclinic	Triclinic	Monoclinic
Space group	$P2_1/c$	$Pna2_1$	$Pna2_1$	$P2_1/c$	$P\bar{1}$	$P\bar{1}$	$P\bar{1}$	$P2_1/c$
a/Å	6.301(2)	26.142(8)	26.009(15)	9.759(5)	9.830(6)	11.032(6)	9.049(4)	17.903(18)
b/Å	29.064(4)	10.442(3)	10.354(3)	15.821(4)	12.202(7)	11.704(4)	11.144(5)	18.445(15)
c/Å	12.661(4)	10.284(3)	10.268(3)	28.626(19)	12.865(8)	13.306(6)	14.023(5)	17.806(28)
α/°	90	90	90	90	107.78(3)	90.74(3)	112.54(2)	90
β/°	92.57(1)	90	90	103.95(3)	92.45(4)	110.90(3)	100.09(2)	91.71(5)
γ/°	90	90	90	90	95.74(3)	117.83(2)	90.97(3)	90
V/Å^3	2316.3(9)	2807(1)	2765(2)	4289(4)	1458(1)	1385(1)	1280.4(9)	5877(12)
Z	4	4	4	4	2	2	2	2
μ/mm^{-1} (radiation)	0.597 (Cu-Kα)	0.676 (Mo-Kα)	0.773 (Mo-Kα)	0.504 (Mo-Kα)	0.892 (Mo-Kα)	1.014 (Mo-Kα)	1.221 (Mo-Kα)	0.807 (Mo-Kα)
Reflections collected	3773	2624	2583	7683	4527	5088	4595	5692
R_{merge} (no. of equiv. reflections)	0.014 (349)			0.016 (163)	0.014 (234)	0.012 (230)	0.009 (107)	0.010 (229)
Observed reflections [$I/\sigma(I) > 2$]	1924	1771	2069	2069	2945	3662	3610	3261
No. of parameters	192	183	183	243	213	186	180	307
Observed reflections/no. parameters	10.0	9.7	11.3	8.5	13.8	19.7	20.1	10.6
Final R, R_w [$I/\sigma(I) > 2$]	0.044, 0.054	0.032, 0.038	0.035, 0.041	0.052, 0.057	0.052, 0.063	0.049, 0.072	0.034, 0.051	0.060, 0.088

References and notes

1 G. Anderegg and F. Wenk, *Helv. Chim. Acta*, 1967, **50**, 2330.

2 (*a*) J. B. Mandel, C. Maricondi and B. E. Douglas, *Inorg. Chem.*, 1988, **27**, 2990; (*b*) G. J. Colpas, B. J. Hamstra, J. W. Kampf and V. L. Pecoraro, *J. Am. Chem. Soc.*, 1996, **118**, 3469; (*c*) R. A. Holwerda, B. R. Whittlesey and M. J. Nilges, *Inorg. Chem.*, 1998, **37**, 64; (*d*) H. Toftlund, S. Larsen and K. S. Murray, *Inorg. Chem.*, 1991, **30**, 3964; (*e*) K. Shiren, S. Fujinami, M. Suzuki and A. Uehara, *Inorg. Chem.*, 2002, **41**, 1598; (*f*) R. A. Holwerda, *Inorg. Chim. Acta*, 1996, **242**, 1; (*g*) M. Krom, R. G. E. Coumans, J. M. M. Smits and A. W. Gal, *Angew. Chem., Int. Ed.*, 2002, **41**, 575; (*h*) K. Shiren, S. Ogo, S. Fujinami, H. Hayashi, M. Suzuki, A. Uehara, Y. Watanabe and Y. Moro-oka, *J. Am. Chem. Soc.*, 2000, **122**, 254; (*i*) Z. He, J. Chaimungkalanont, D. C. Craig and S. B. Colbran, *J. Chem. Soc., Dalton Trans.*, 2000, 1419; (*j*) H. Sugimoto, C. Matsunami, C. Koshi, M. Yamasaki, K. Umakoshi and Y. Sasaki, *Bull. Chem. Soc. Jpn.*, 2001, **74**, 2091; (*k*) K. Jitsukawa, Y. Oka, H. Einaga and H. Masuda, *Tetrahedron Lett.*, 2001, **42**, 3467; (*l*) T. Kojima and Y. Matsuda, *J. Chem. Soc., Dalton Trans.*, 2001, 958; (*m*) T. Kojima, T. Amano, Y. Ishii, M. Ohba, Y. Okaue and Y. Matsuda, *Inorg. Chem.*, 1998, **37**, 4076; (*n*) R. M. Chin, R. H. Dubois, L. E. Helberg, M. Sabat, T. Y. Bartucz, A. J. Lough, R. H. Morris and W. D. Harman, *Inorg. Chem.*, 1997, **36**, 3553; (*o*) Y. Bretonniere, M. Mazzanti, J. Pecaut, F. A. Dunand and A. E. Merbach, *Inorg. Chem.*, 2001, **40**, 6737; (*p*) R. Wietzke, M. Mazzanti, J.-M. Latour and J. Pecaut, *J. Chem. Soc., Dalton Trans.*, 2000, 4167; (*q*) A. Hazell, J. McGinley and H. Toftlund, *J. Chem. Soc., Dalton Trans.*, 1999, 1271; (*r*) R. Wietzke, M. Mazzanti, J.-M. Latour, J. Pecaut, P.-Y. Cordier and C. Madic, *Inorg. Chem.*, 1998, **37**, 6690.

3 K. Chen, M. Costas and L. Que, Jr., *J. Chem. Soc., Dalton Trans.*, 2002, 672.

4 L. Que, Jr. and W. B. Tolman, *Angew. Chem., Int. Ed.*, 2002, **41**, 1114.

5 K. D. Karlin, S. Kaderli and A. D. Zuberbuhler, *Acc. Chem. Res.*, 1997, **30**, 139.

6 M.-A. Kopf and K. D. Karlin, in *Biomimetic Oxidations Catalyzed by Transition Metal Complexes*, ed. B. Meunier, Imperial College Press, London, 1999, pp. 309–362.

7 Y. Zang, J. Kim, Y. H. Dong, E. C. Wilkinson, E. H. Appelman and L. Que, Jr., *J. Am. Chem. Soc.*, 1997, **119**, 4197.

8 H. Hayashi, S. Fujinami, S. Nagatomo, S. Ogo, M. Suzuki, A. Uehara, Y. Watanabe and T. Kitagawa, *J. Am. Chem. Soc.*, 2000, **122**, 2124.

9 H. Hayashi, K. Uozumi, S. Fujinami, S. Nagatomo, K. Shiren, H. Furutachi, M. Suzuki, A. Uehara and T. Kitagawa, *Chem. Lett.*, 2002, 416.

10 K. D. Karlin, J. C. Hayes, S. Juen, J. P. Hutchinson and J. Zubieta, *Inorg. Chem.*, 1982, **21**, 4106.

11 H. Nagao, N. Komeda, M. Mukaida, M. Suzuki and K. Tanaka, *Inorg. Chem.*, 1996, **35**, 6809.

12 C. L. Chuang, K. T. Lim and J. W. Canary, *Supramol. Chem.*, 1995, **5**, 39.

13 C. L. Chuang, K. Lim, Q. Chen, J. Zubieta and J. W. Canary, *Inorg. Chem.*, 1995, **34**, 2562.

14 C. L. Chuang, O. Dossantos, X. D. Xu and J. W. Canary, *Inorg. Chem.*, 1997, **36**, 1967.

15 J. W. Canary, C. S. Allen, J. M. Castagnetto, Y.-H. Chiu, P. J. Toscano and Y. Wang, *Inorg. Chem.*, 1998, **37**, 6255.

16 S. J. Lange, H. Miyake and L. Que, Jr., *J. Am. Chem. Soc.*, 1999, **121**, 6330.

17 D. Mandon, A. Nopper, T. Litrol and S. Goetz, *Inorg. Chem.*, 2001, **40**, 4803.

18 Z. He, S. B. Colbran and D. C. Craig, *Chem. Eur. J.*, 2002, in press.

19 D. F. Xiang, C. Y. Duan, X. S. Tan, Y. J. Liu and W. X. Tang, *Polyhedron*, 1998, **17**, 2647.

20 S. Menage, Y. Zang, M. P. Hendrich and L. Que, Jr., *J. Am. Chem. Soc.*, 1992, **114**, 7786.

21 Y. M. Chiou and L. Que, Jr., *J. Am. Chem. Soc.*, 1995, **117**, 3999.

22 Y. Zang, H. G. Jang, Y. M. Chiou, M. P. Hendrich and L. Que, Jr., *Inorg. Chim. Acta*, 1993, **213**, 41.

23 C. S. Allen, C.-L. Chuang, M. Cornebise and J. W. Canary, *Inorg. Chim. Acta*, 1995, **239**, 29.

24 G. Hilt, T. Jarbawi, W. R. Heineman and E. Steckhan, *Chem. Eur. J.*, 1997, **3**, 79.

25 A. Nanthakumar, S. Fox, N. N. Murthy and K. D. Karlin, *J. Am. Chem. Soc.*, 1997, **119**, 3898.

26 Z. H. Zhang, X. H. Bu, Z. A. Zhu, Z. H. Jiang and Y. T. Chen, *Transition Met. Chem.*, 1996, **21**, 235.

27 R. H. Bode, W. L. Driessen, F. B. Hulsbergen, J. Reedijk and A. L. Spek, *Eur. J. Inorg. Chem.*, 1999, 505.

28 Z. Tyeklar, P. P. Paul, R. R. Jacobson, A. Farooq, K. D. Karlin and J. Zubieta, *J. Am. Chem. Soc.*, 1989, **111**, 388.
29 N. N. Murthy and K. D. Karlin, *J. Chem. Soc., Chem. Commun.*, 1993, 1236.
30 H. Adams, N. A. Bailey, D. E. Fenton and Q.-Y. He, *J. Chem. Soc., Dalton Trans.*, 1997, 1533.
31 M. M. da Mota, J. Rodgers and S. M. Nelson, *J. Chem. Soc. A*, 1969, 2036.
32 B. Tong, S. C. Chang, E. E. Carpenter, C. J. O'Connor, J. O. Lay, Jr. and R. E. Norman, *Inorg. Chim. Acta*, 2000, **300–302**, 855.
33 The trigonality index (τ) for five-coordinate complexes is 1 for a trigonal bipyramid and 0 for a square-based pyramid: A. W. Addison, A. N. Rao, J. Reedjik, J. Rijn and G. C. Verschoor, *J. Chem. Soc., Dalton Trans.*, 1984, 1349.
34 A. B. P. Lever and E. I. Solomon, in *Ligand-Field Theory & the Properties of Transition Metal Complexes*, eds. A. B. P. Lever and E. I. Solomon, J. Wiley and Sons, New York, 1999, vol. 1, pp. 1–92.
35 M. Ciampolini and N. Nardi, *Inorg. Chem.*, 1966, **5**, 41.
36 P. L. Orioli, *Coord. Chem. Rev.*, 1971, **6**, 285.
37 In other 'Ni(II)($R_n$tpa)X_2' ($R_n$tpa = 6-alkyl substituted tpa-derivative; X = halide) compounds, five-coordinate species with a N_4Cl donor set exhibit spectra in which ν_1 and ν_2 appear at higher energy, ν_3 has a prominent high energy shoulder and there is a prominent peak at 20,000 cm^{-1}; the spectrum of octahedral [Ni(tpa)Cl_2] is different again, displaying symmetric weak bands at 9,800 cm^{-1} and 15,800 cm^{-1} with a third higher energy band at ~27,000 cm^{-1} apparent as shoulder to an intense ligand-centred band. See refs. 31 and 32.
38 M. Schatz, M. Becker, F. Thaler, F. Hampel, S. Schindler, R. R. Jacobson, Z. Tyeklar, N. N. Murthy, P. Ghosh, Q. Chen, J. Zubieta and K. D. Karlin, *Inorg. Chem.*, 2001, **40**, 2312.
39 J. Sandström, *Dynamic NMR Spectroscopy*, Academic Press, London, 1982.
40 H. Kessler, *Angew. Chem., Int. Ed. Engl.*, 1970, **9**, 219.
41 M. J. S. Dewar and W. B. Jennings, *J. Am. Chem. Soc.*, 1971, **93**, 401.
42 V. Amendola, L. Fabbrizzi, C. Mangano and P. Pallavicini, *Struct. Bonding (Berlin)*, 2001, **99**, 79.
43 R. D. Shannon, *Acta Crystallogr., Sect. A*, 1976, **32**, 751.